Materials Physics and Mechanics. 2023;51(3): 146-166
Research article
http://dx.doi.org/10.18149/MPM.5132023_15

Submitted: January 23, 2023
Approved: February 27, 2023
Accepted: March 20, 2023

Modeling of delamination process coupling contact, friction, and adhesion considering the thermal effect

Abdellah Benchekkour [1] ✉, Nazihe Terfaya [2], Mohammed Elmir[3], Tayeb Kebir [4,5], Mohamed Benguediab [5]

[1] ENERGARID Laboratory, Tahri Mohammed University, Bechar, Algeria

[2] FIMAS Laboratory, Tahri Mohammed University, Bechar, Algeria

[3] L2ME Laboratory, Tahri Mohammed University, Bechar, Algeria

[4] Department of Technical Sciences, Institute of Science and Technology, University Center Salhi Ahmed, Naama, Algeria

[5] Laboratory of Materials and Systems Reactive, Faculty of Technology, University of Sidi Bel Abbes, Algeria

✉ benchekkour.abdellah@univ-bechar.dz

Abstract. The main objective of this work is based on a numerical study of delamination behavior between an elastic body and a rigid support, taking into account the thermal effect. A cohesive zone model (CZM) coupling friction and adhesion is used and implemented in the finite element software ABAQUS which allows to gives a smooth transition from total adhesion to the usual Coulomb friction law with unilateral contact, where adhesion is regarded as interface damage. Also, a sequentially coupled thermal stress model is performed to predict the thermomechanical behavior assuming a steady-state thermal analysis. The influence of the decohesion energy, the interface initial stiffnesses, and friction coefficient are analyzed. The results showed that the thermal effect is not negligible and can affect the delamination process in failure modes I and II. The proposed numerical model is in good agreement with the results compared to those obtained in the literature.

Keywords: delamination, unilateral contact, coulomb friction law, cohesive zone model, finite element method, thermal effect

Acknowledgements. *The authors gratefully acknowledge the ENERGARID Lab and FIMAS Lab at UTM Bechar University, for computational resources, and to provide technical guidance during this study.*

Citation: Benchekkour A, Terfaya N, Elmir M, Kebir T, Benguediab M. Modeling of delamination process coupling contact, friction, and adhesion considering the thermal effect. *Materials Physics and Mechanics*. 2023;51(3): 146-166. DOI: 10.18149/MPM.5132023_15.

Introduction

Delamination problems are one of the most challenging engineering problems, and represent the most critical modes of damage. The presence of such problems in structures and materials weakens their reliability and increases the cost and time of maintenance and repair. Therefore, the prediction of delamination is essential to analyze the failure process. Originally, this problem is often confronted with more complex physical behaviors (contact, friction, and thermal effect.). For this complexity, we must model this multi-physical problem with an effective computational tool. In general, the most used approaches to solve fracture problems

© A. Benchekkour, N. Terfaya, M. Elmir, T. Kebir, M. Benguediab, 2023.
Publisher: Peter the Great St. Petersburg Polytechnic University
This is an open access article under the CC BY-NC 4.0 license (https://creativecommons.org/li-censes/by-nc/4.0/)

are the cohesive zone model (CZM) and linear elastic fracture mechanics (LEFM). The CZM has proven a useful tool compared to linear elastic fracture mechanics LEFM methods for solving contact and fracture problems and can be applied to more physical coupling phenomena such as the thermal effect [1]. CZM describes the relationship between cohesive tractions along the interface (also known as the contact surface) and the displacements jump by the traction separation law (TSL). There are different shapes of TSL (also known as cohesive law), such as bi-linear, exponential, cubic polynomial, and trapezoidal shapes. The choice of TSL is dependent on the problem at hand, such as the type of materials and fracture process [2]. In addition, there are three techniques to model the delamination with CZM: interface elements, contact elements, or a User-defined Elements (UEL) [3], these techniques are used on several delamination problems, such as the delamination in composite materials [4], in adhesive bond joints (debonding) [5,6], delamination of surfaces in contact (bi-material interface delamination) [7] and the damage of composite patch [8]. As we mentioned above, the delamination phenomena are subjected to more different physical problems in reality, such contact and friction behaviors after debonding. In this context, many authors have touched on this coupled problem between damage, contact, and friction such as [9–14]. Especially, the works of Raous and Terfaya on the delamination in modes I and II [15–21]. On the other hand, the presence of a thermal field is not negligible and can affect the delamination mechanism. So, it is important to take into account these phenomena for an optimal and realistic prediction of delamination behavior.

According to the literature, there are several studieson the delamination behavior under thermal effect using the CZM approach. Li et al. [22] studied the fracture behavior of asphalt mixtures at low temperatures using the interface element technique. Białas et al. [23] presented a numerical simulation of the interfacial crack of the oxide/ceramic interface subjected to temperature loading. Nikolova et al. [24] analyzed a bi-material elastic isotropic plate bonded by an interface under thermal loading. Chen et al. [25] used a modified cohesive model to investigate a multi-delamination of composite T-piece specimens under mixed mode loading taking into account the thermal effect. Ho et al. [26] modeled the Interfacial delamination between the pad and the encapsulant in microelectronic packaging under thermal loading. Moreover, different works studied the interfacial fracture under thermal effect in Refs. [27-30].

Recently, Im et al. [31] predicted the progressive failure behavior to evaluate the effect of temperature on the adhesive joining of a domeseparated composite pressure vessel through Mode I, Mode II, and Mixed Mode I/II interfacial fracture toughness tests. Jiang et al. [32] studied the interfacial cracking between the ceramic top coat and the metallic bond coat under cyclic thermal loading. Na et al. [33] investigated the effect of temperature on the mechanical properties of adhesively bonded basalt FRP-aluminum alloy joints at different temperatures. Yang et al. [34] studied the Interfacial shear failure and large longitudinal displacement under temperature load. He et al. [35] investigated the effect of moderately elevated temperatures on the bond behavior of CFRP-to-steel bonded joints using different adhesives. Chen et al. [36] studied the interface damage between the cement concrete base plate and asphalt concrete waterproofing layer under temperature load via experimental and simulation analysis. Katafiasz et al. [37] examined the influence of temperature and moisture on the mode I of the interlaminar fracture of a carbon fiber/epoxy composite material, Cui et al. [38] developed a three-dimensional (3D) finite element model to study the interface damage and the arching deformation of China railway track system (CRTS) II slab track under high-temperature conditions. Furthermore, Guo et al. [39] analyzed the effect of thermal stress on the debonding failure of Fiber-reinforced polymer strengthened steel beams. Also, Gong et al. [40] investigated the effects of temperature on the delamination growth process in mode I. The delamination growth behavior of curved composite laminates at elevated temperatures, examined by Truong et al. [41]. While in [42,43], the authors studied the damage interfacial

under thermal effect coupled with others techniques, such as Molecular dynamics simulations technique [42], and continuum damage [43].

For the fracture and contact problems under thermal effect, Erdogan and Wu [44] studied a crack/contact problem in a functionally graded material (FGM) layer under thermal stresses. Chen [45] investigated a 3D crack and contact analysis of advanced materials coupling between the temperature field and other physical fields. Based on the literature, it is noted that many researchers have studied the effect of temperatures on delamination behavior. However, the behavior of delamination in the presence of a thermal field, taking into account the unilateral contact and Coulomb's law of friction, has not been studied in a thorough and detailed manner. Therefore, the current article will cover this point and present a finite element modeling of interface delamination phenomena under different thermal loading using a cohesive model coupling contact, friction, and adhesion. This insures a continuous transition between the total adhesive and pure frictional states. The Coulomb friction law with unilateral contact (Signorini conditions) is considered. For the thermal analysis, a steady state is adopted. To simulate the thermal effect on delamination, sequentially thermal stress analysis was performed. The study was carried out on benchmarks using the FE ABAQUS software. The problem was solved by considering delamination in modes I and II.

Mathematical formulation

In this work, a Multiphysics coupling problem is discussed, we are interested in the contact two-dimensional and fracture problem in the presence of the thermal field. The contact problem is a Signorini problem (strictly unilateral conditions) with Coulomb friction law. The fracture problem modeled with the cohesive zone model coupling contact, friction, and adhesion; these models allow the simulation of the fracture problem of solids as well as the interfaces between them. These problems are characterized by a non-regular boundary condition and can be formulated with evolutionary variational inequations or differential inclusions. In addition, for the thermomechanical coupling, a weak coupling or sequentially coupled thermal-stress, is used.

Unilateral contact and coulomb friction laws. In this section, most often used of contact and friction laws are first presented before giving the basic formulation of frictional unilateral contact. In the contact laws, we have unilateral and bilateral contact. Consider a system consisting of two solids A and B in contact. If in all the possible positions of the system there is contact between the solids, the liaison is said to be bilateral. If on the contrary, among the possible positions of the system there are positions with contact and others without; the liaison is said to be unilateral. We note that unilateral contact as opposed to bilateral contact. Two bodies in bilateral contact cannot separate, they can only slide against each other [46]. Here, we focus on the unilateral contact, which take into account the non penetration of the solids in contact. Before presenting the Signorini conditions problem, a kinematic description to formulate the contact problem are defined as shown at Fig. 1 [17]. Let A and B be two deformable solids in contact, with $\boldsymbol{\Gamma_c}$ the common contact surface. We denote x_n the shortest magnitude of the normal coordinate between two solids in contact, and $(\vec{n}, \vec{t}_1, \vec{t}_2)$, $\vec{n}$ denote respectively the local coordinate system, and the normal unit vector at point P' to the bodies, directed towards A. $T(\overrightarrow{t_1}, \overrightarrow{t_2})$ denotes the orthogonal plane to $\vec{n}$ in $\Re^3$.

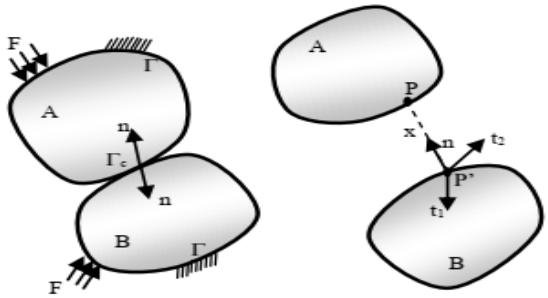

Fig. 1. Kinematics of contact

We obtain the decomposition of the contact reaction and relative velocity in the following form:

$$\dot{\boldsymbol{u}} = \dot{\boldsymbol{u}}_{\boldsymbol{t}} + \dot{u}_n \boldsymbol{n}$$
$$\boldsymbol{R} = \boldsymbol{R}_{\boldsymbol{t}} + R_n \boldsymbol{n}' \quad (1)$$

where R_n, R_t respectively the contact force and the friction force, and $\dot{u}_n$, $\dot{u}_t$ respectively is the normal relative velocity and the sliding velocity. These variables define the unilateral contact conditions or known as the Signorini conditions, and which can be written as follow [20,47,48]:

$$x_n \geq 0; R_n \geq 0; \; and \; R_n x_n = 0. \quad (2)$$

From this expression, we have three different possible conditions: a kinematic condition (non-penetration $x_n = 0$, a static condition (non-adhesion $R_n \geq 0$ and mechanical complementarity condition (non-contact $R_n x_n = 0$). Under consideration the initial gab h_0 between the bodies A and B, with:

$$x_n = h_0 + u_n. \quad (3)$$

The condition of Signorini problem is written as follow:

$$u_n \geq 0; R_n \geq 0; \; and \; R_n u_n = 0. \quad (4)$$

When two bodies into contact with each other ($u_n = 0$), from this condition, we directly express the unilateral contact law (Signorini's conditions) in terms of velocity [20,47,48]:

$$\dot{u}_n \geq 0; R_n \geq 0; \; and \; R_n \dot{u}_n = 0. \quad (5)$$

In the friction laws, there are several models in the literature, here we give the most frequently used, Coulomb and Tresca laws. The cause of the similarity of Tresca law with the corresponding plasticity law is often used. Moreover, and only when the normal pressure is known and constant will this law be applicable. Hence, the friction threshold is fixed in advance in this law. It cannot be written directly with unilateral contact because the normal force is unknown a priori. Therefore, we focus only on the coulomb law, where the friction threshold is proportional to the normal contact force. Coulomb's law is the most commonly used because it is simpler, more efficient, and more realistic than other laws. The coulomb model friction is written [20,47,48]:

$$\begin{cases} \|R_t\| \leq \mu \cdot R_n \;\; if \quad u_t = 0 \\ \|R_t\| = -\mu \cdot R_n \frac{\dot{u}_t}{\|\dot{u}_t\|} \;\; if \; \dot{u}_t \neq 0 \end{cases}' \quad (6)$$

where μ is the friction coefficient of the coulomb law. Thus, we formulate the isotropic coulomb cone K_μ as shown:

$$K_\mu = \{R \in \Re \; such \; that \; f(R) = \|R_t\| - \mu R_n \leq 0\}. \quad (7)$$

In the case of the frictional contact law, we combine the Signorini condition to the coulomb law to make the problem well posed. This law describes the interface behavior and can be divided into two different cases. In the first, when the contact occurs, each pair of contact points belonging to the interface can be in one of the two states: sticking or sliding [49].

For the state of sticking:

$$R \in K_\mu, \|R_t\| \leq \mu R_n \; and \; \dot{u} = 0. \quad (8)$$

For the state of sliding:

$$R \in K_\mu, and\ \|R_t\| = -\mu \cdot R_n \frac{\dot{u}_t}{\|\dot{u}_t\|}\ \ if\ \dot{u}_t \neq 0. \quad (9)$$

In the second case, the state of no contact, when two bodies separate:

$$R_n = 0, and\ \ \dot{u}_n \geq 0. \quad (10)$$

Cohesive zone modeling. Usually for solving fracture problems, two theories are distinguished: linear elastic fracture mechanics (LEFM) and cohesive zone models (CZM). LEFM is a popular tool for simulating the fracture process. However, it cannot be applicable in all cases due to its limitation in some complex problems. The most severe limitations of LEFM are its inability to predict: the crack initiation, the temporal evolution of the cracks (instabilities), spatial evolutions (bifurcation, branching), and not take into account the non-linearities induced by the deformations of the crack front and also the conditions of the complex problem (contact, friction) on the crack surfaces [50]. This is why it is important to use CZM.

The CZM is a very widely used to predict fracture and damage processes in materials for the reason of their success with a large range of materials and they can be applied to various fracture processes (ductile fracture, dynamic fracture, fatigue, etc..) and they can be coupled easily with more complex problems (contact, friction, thermal, corrosion, etc.…). Significantly, it is the most tool commonly used to model bi-material interface behavior. Therefore, it's used for interlaminar fractures such as delamination [51].

The CZM considers fracture formation as a gradual phenomenon, and its concept is based on the notion of the cohesive zone or the fracture nonlinear process zone when material damage is introduced. This model is described by a relation between the cohesive stresses vector $\boldsymbol{\sigma^{coh}}$ and the displacement jump δ between the crack surfaces as shown in Fig. 2. Originally, this notion was introduced by Dugdale (1960) [52], Barenblatt (1962) [53]. Moreover, this behavior is characterized by four stages. In the first stage I of the fracture process, the material behavior is characterized without damage. Then, the second stage II is the initiation of a crack, when increasing separation δ the traction σ^{coh} increases and reaches maximum stress (cohesive strength $\sigma^{coh}{}_{max}$). The third stage III describes the damage evolution when the traction across the interface decreases and eventually vanishes at the critical separation, then defines the failure zone or the fourth IV and last stage when creating the new crack surfaces with no traction forces [54].

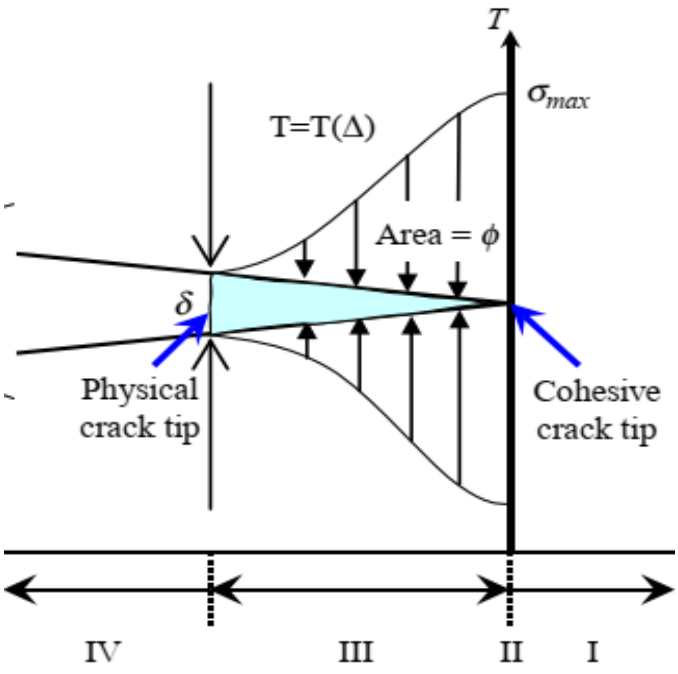

Fig. 2. Cohesive zone mode. Based on [51]

The traction-separation law (TSL) or the cohesive law describes irreversible phenomena such as damage. The form of TSL (bilinear, linear-parabolic, exponential, and trapezoidal) defines the initiation and the evolution of damage, and it plays a very critical role in determining the failure behavior [2]. In the framework of finite elements simulation, CZM is a powerful and efficient computational method for solving fracture problems, in this case, CZM is implemented numerically via commercial software ABAQUS. The separation mechanism of the two surfaces can be simulated using three techniques in ABAQUS: interface elements, contact elements or a User defined Elements (UEL). In our study, we focus on delamination phenomena along an interface between two solids, taking into account the problem of contact with friction. Interface delamination modeled with CZM using a bilinear cohesive model and contact elements technique. The TSL in ABAQUS describes a relationship between the traction $\boldsymbol{\sigma^{coh}}$ on the interface and the corresponding interfacial separation or displacement jump δ. a displacement jump is defined as:

$$\delta = \frac{P \cdot L}{A \cdot E}, \tag{11}$$

where L the displacement of a truss of length, E elastic stiffness, and A original area due to an axial load P. With δ is separated into two parameters, δ_n normal separation and δ_t tangential separation as follow:

$$\boldsymbol{\delta_n} = \delta . \boldsymbol{n}$$
$$\boldsymbol{\delta_t} = \delta . \boldsymbol{t} . \tag{12}$$

The vector of nominal traction $\boldsymbol{\sigma^{coh}}$ consists of two components in two-dimensional problems ($\boldsymbol{\sigma_n^{coh}}$, $\boldsymbol{\sigma_t^{coh}}$) the corresponding separations are denoted by δ_n, and δ_t. The elastic behavior can then be written as [3]:

$$\sigma^{Coh} = \begin{Bmatrix} \sigma^{Coh}{}_n \\ \sigma^{Coh}{}_t \end{Bmatrix} = \begin{pmatrix} K_{nn} & K_{nt} \\ K_{nt} & K_{tt} \end{pmatrix} \begin{Bmatrix} \delta_n \\ \delta_t \end{Bmatrix} = K\delta, \tag{13}$$

where K_{nn} and K_{tt} is the normal and tangential contact stiffness. In the bilinear cohesive zone material model, the initial response of the interface is assumed to be linear up to the maximum traction stress. Then, is followed by linear softening and when the contact stress reaches zero value, the interface is fully damaged and one finds the classical contact laws. The area under the curve is the energy released due to delamination and is called the critical fracture energy, as shown in Fig. 3. In the finite element simulation, the critical fracture energy and the maximal cohesive stress are the essential parameters for defining TSL.

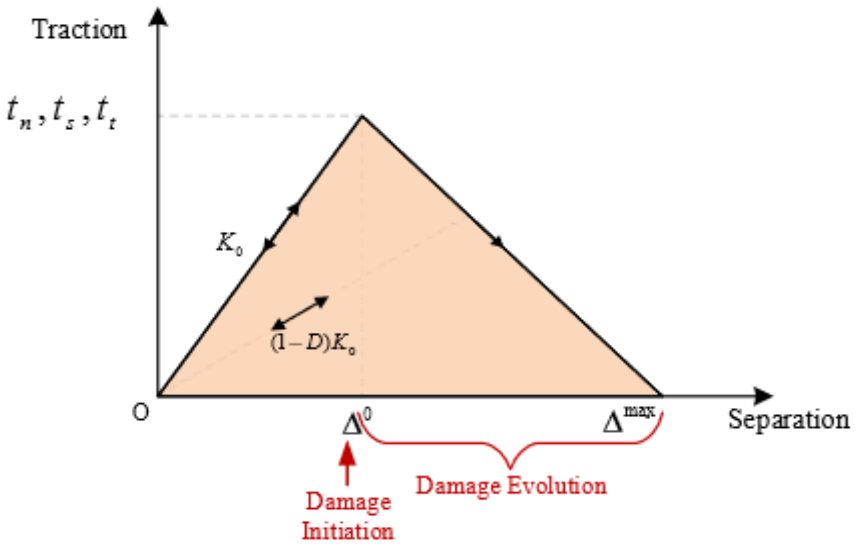

Fig. 3. Typical Bilinear Traction-Separation response. Based on [3]

The damage initiation refers to the beginning of the delamination. The process of delamination begins when the stresses satisfy certain damage initiation criteria, several damage initiation criteria are available, in this case we use maximum nominal stress criterion [3]:

$$max\left\{\frac{\langle \sigma^{Coh}{}_n \rangle}{\sigma^{Coh}{}_n{}^0}, \frac{\sigma^{Coh}{}_t}{\sigma^{Coh}{}_t{}^0}\right\} = 1. \quad (14)$$

We denote $\sigma^{Coh}{}_n{}^0$ and $\sigma^{Coh}{}_t{}^0$ respectively the peak values of the nominal stress when the deformation is either purely normal to the interface or purely in the first or the second shear direction. In addition, damage evolution describes the interface degradation once the corresponding damage initiation criterion is reached, and defined by scalar damage D, with D monotonically evolves from 0 to 1, which are given as [3]:

$$\sigma^{coh} = (1 - D)\overline{\sigma^{coh}}, \quad (15)$$

where $\overline{\sigma^{coh}}$ denoted the stress tensor computed in the current increment without damage. Damage evolution is based on the displacement or energy, in the present work we use energy criteria. The area under the TSL curve equals the fracture energy, the power law criterion is given by:

$$\left\{\frac{G_n}{G_n^c}\right\}^\alpha + \left\{\frac{G_t}{G_t^c}\right\}^\alpha = 1. \quad (16)$$

We denote G_n and G_t respectively, the work done by the tractions and their conjugate relative displacements in the normal and shear directions, and G_n^c and G_t^c respectively, the critical fracture energies required to cause failure in the normal, the first, and the second shear directions.

Numerically, the major difficulty of CZM is the convergence problem due to the solution jumps. To remedy this problem, we introduce a viscous regularization (b) [55].

Coupling contact, friction, and adhesion. This part is concerned with the coupling of contact, friction, and adhesion in interface delamination modeling such as the works of Raous and Terfaya [15-20]. The Signorini problem with coulomb friction law is strictly imposed and coupled to adhesion. The adhesion part of this coupling is inspired by the CZM using the contact element technique. According to this coupling model, the total force R^{total} can be expressed as the sum of the cohesive force R^{coh} and the contact force R^{cont}:

$$R^{total} = R^{cont} + R^{Coh}. \quad (17)$$

According to the previous equation, the global force can be expressed into normal and tangential components.

The coupling between unilateral conditions with adhesion:

$$R_n{}^{total} = R_n{}^{cont} + R_n{}^{Coh}. \quad (18)$$

With R_n^{total}, R_n^{cont} and R_n^{coh} respectively the total normal force, the normal contact force and the cohesive normal force. We directly express the coupling between unilateral conditions with adhesion in terms of stresses:

$$\sigma_n{}^{total} = \sigma_n{}^{cont} + \sigma_n{}^{Coh}. \quad (19)$$

The coupling between coulomb friction and adhesion:

$$R_t{}^{total} = R_t{}^{cont} + R_t{}^{Coh}. \quad (20)$$

R_t^{total}, R_t^{cont} and R_t^{coh} represent the total, the contact and the cohesive tangential forces respectively. And for the stresses term:

$$\sigma_t{}^{total} = \sigma_t{}^{cont} + \sigma_t{}^{Coh}. \quad (21)$$

Thermomechanical coupling. There are two methods for thermomechanical coupling in ABAQUS. In the first, the sequentially coupled thermal-stress analysis when the stress/displacement solution is dependent on a temperature field but there is no inverse dependency. In this case, the equations are solved sequentially. In the second, the fully coupled thermal-stress analysis when the thermal and mechanical solutions affect each other strongly, also known as a fully-coupled scheme, the governing equations are solved simultaneously [3].

Here, we are interested in the sequentially coupled analysis (weak coupling). The heat conduction equation for a homogeneous and isotropic material with no internal heat source, in two-dimensional case and steady-state analysis is given by:

$$\frac{\partial^2 T}{\partial x^2} + \frac{\partial^2 T}{\partial y^2} = 0. \quad (22)$$

The thermal relative displacement component ε_{th} is written as:

$$\varepsilon_{th} = \alpha \Delta T, \quad (23)$$

where ΔT is the temperature change and α is the coefficient of thermal expansion. The finite element formulation of the steady state equation is written in the following:

$$[\lambda]\{T\} = \{F_{th}\}, \quad (24)$$

where, $[\lambda]$ is the thermal conductivity matrix and $\{F_{th}\}$ is the thermal force vector. The global relative displacement ε, with take into account the thermal effects, is given by:

$$\varepsilon = \varepsilon_{mec} + \varepsilon_{th} \quad (25)$$

Moreover, the finite element formulation for the resolution of the delamination problem under thermal effect coupling contact, friction, and adhesion is obtained:

$$\left[K_g\right]\{U\} = \left\{F_g\right\} + \left\{R_{total\ g}\right\} + \left\{F_{thg}\right\}, \quad (26)$$

where $\left[K_g\right]$, $\{U\}$ and $\left\{F_g\right\}$ are respectively the stiffness matrix, the displacement vector and the force vector.

Finite element simulation

In this article, a few benchmark problems in delamination are solved using a bilinear cohesive model coupling contact, friction and adhesion implemented in the standard finite element software ABAQUS, the node-to-surface contact interaction is used to defined the interface. A steady state thermal analysis is performed. In addition, for the thermo-mechanical coupling, we use sequential thermal-stress analysis. Therefore, the Lagrange multiplier method is used as an approach to solve the problem. To study and to analyze the thermal effect on delamination phenomena, two problems are considered. The problems considered are [15-17]:

1. Delamination of a thin layer of aluminum submitted to vertical loading (mode I);
2. Shear delamination of a block of aluminum (mode II).

These problems are subjected to different thermal loading. In our study, we assume there is no heat exchange at the interface. For this reason and to avoid any thermal conduction, a very low thermal conductivity value was chosen for the rigid support.

Delamination of a thin layer of aluminum submitted to vertical loading

The first example deals with a 2D (*LxH*) plane strain delamination problem under thermal effect, this is a case of interface cracking in mode I. This example poses a delamination problem of a thin layer of Aluminum (Young's modulus E = 69000 MPa, Poisson's ratio ν = 0.333, Thermal Conductivity λ = 230 W/m·k and Expansion Coefficient α = 23E-6/ K) submitted to incrementally vertical loading at point A, this thin layer initially adhered to a rigid support. The maximum value of the vertical displacement is V = 0.3 mm (in 1 sec). The geometric configuration and boundary conditions are shown in Fig. 4, with L = 50 mm; H = 2.5 mm.

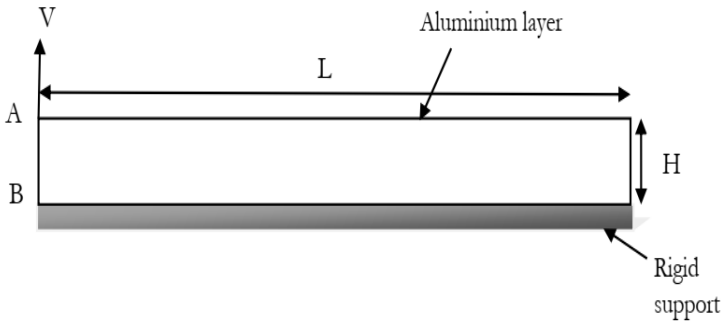

Fig. 4. Geometry and boundary conditions

The interface properties are summarized in Table 1, in which the interface behavior is considered with dissipative law ($b \neq 0$). In the first instance, we suppose that we have zero displacement ($u_n = u_t = 0$) and no damage ($D = 0$).

Table 1. The interface properties

Properties	The decohesion energy w, mJ/mm^2	The maximal cohesive stress $\sigma^{coh}{}_{max}$, MPa	The initial stiffnesses of the interface K_{nn}, K_{tt}, MPa/mm	The interface viscosity b, Ns/mm	The friction coefficient μ
Interface	10E-6	0.0114	2.E+5	0.09	0.2

Mesh convergence test. Due to the contact problem between a deformable body and a rigid foundation, the geometry has been discretized with a linear triangular element as known in the literature. In addition, we are interested in solving the interface problem with node-to-surface contact interaction. For this purpose, we study the mesh convergence with a different number of elements (10, 32 and 40 elements) to choose the optimum mesh element that is capable to predict the realistic delamination mechanism. Figure 5 represents the debonding evolution along the interface with different finite elements numbers.

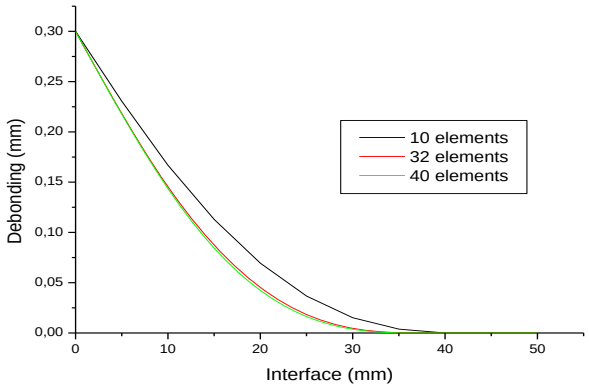

Fig. 5. The debonding evolution along the interface

In this study and as we mentioned above the contact is defined by node-to-surface interaction. Therefore, we chose a linear triangular element. For comparison purpose, we use the element type (CPE3: A 3-node linear plane strain triangle). The results indicate the

difference between the element number (32 and 40) is negligible, but in the case of 10 elements, the result is different. Therefore, CPE3 32 elements and 33 contact nodes in the interface was adopted as for accurate results as the work of Terfaya [15-17]. The deformed meshes is shown in Fig. 6 for three-time steps t1, t2, and t3.

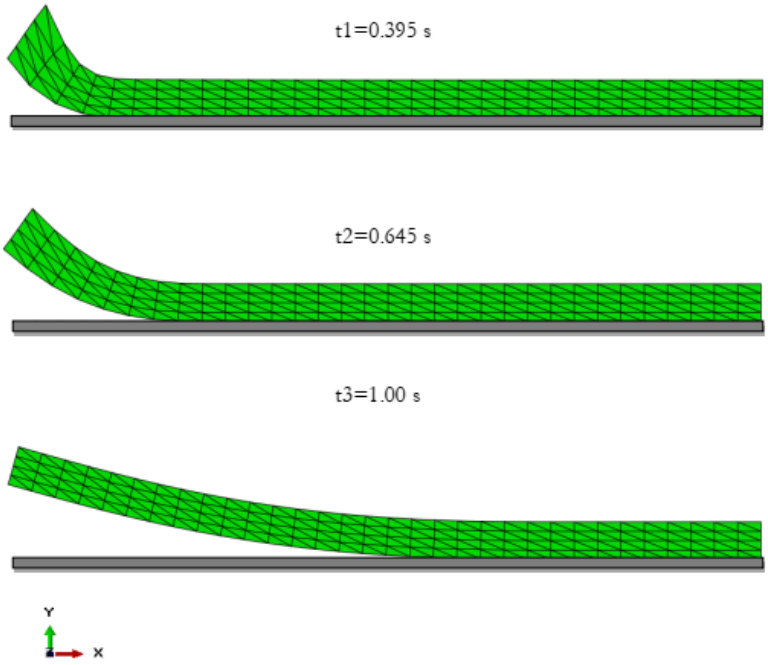

Fig. 6. The deformed meshes

The three diagrams characterize the interfacial crack propagation under the effect of normal loading. At the beginning of loading, a debonding at the point B is clearly observed. This case is the opening mode (mode I). The interface fracture starts to increase when the normal total stress σ_n^{tot} decreases until equal to zero at the interface and we find Signorini's classic law.

Temperature effect. In order to evaluate the temperature effect, two different cases have been studied:

1. Case 1: four states of imposed temperature on the upper face of the thin layer with T_{sup}=25, 50, 75 and 100 °C and on the right lateral edge of the thin layer a temperature imposed constant T_{rght} = 50 °C.
2. Case 2: a temperature imposed constant T_{sup} = 50 °C on the upper face of the thin layer and an imposed temperature on the right lateral edge of the thin layer with T_{rght} = 25, 50, 75 and 100 °C, for all states.

For the case 1, the normal displacement u_n along the interface with and without the thermal effect is shown in Fig. 7(a). One can easily notice that the debonding decreases, and the behavior of the interface is significantly affected by the presence of the thermal field. In order to enrich the study of delamination on mode I, we reported on Fig. 7(b), the evolution of the normal stresses σ_n^{total} at point B as a function of debonding u_n with and without the thermal effect. The influence of the temperature on the delamination behavior is reflected in the different thermal conditions considered. Under the imposed displacement, an adhesive resistance R_n^{coh} is mobilized, and added to the normal contact reaction (elasticity with damage). As long as the energy threshold (w) is unreached, adhesion stays to be complete the behavior

of the interface is elastic, and unaffected by the presence of thermal stress. The delamination starts to increase when the displacement is sufficiently large such that the elastic energy becomes larger than the limit of adhesion energy (w). At this stage, the thermal field affects the interface behavior. It can be noted that the presence of the thermal stress causes an accelerated delamination, expressed by the diminution of the maximal total normal stress $\sigma_n^{total}{}_{max}$. This is mainly due to the slip caused by the dilatancy. When delamination is total, the cohesive reactions tend to zero, and the classical Signorini problem is obtained. In addition, we determine the delamination process parameters such as the total energy dissipated during crack propagation, the maximal total normal stress, the opening displacement at the maximum total normal stress and maximum opening displacement as illustrated in Table 2. The first observation is that all the delamination parameters decrease when the temperature is increased, which proves the delamination accelerated in the presence of a thermal field.

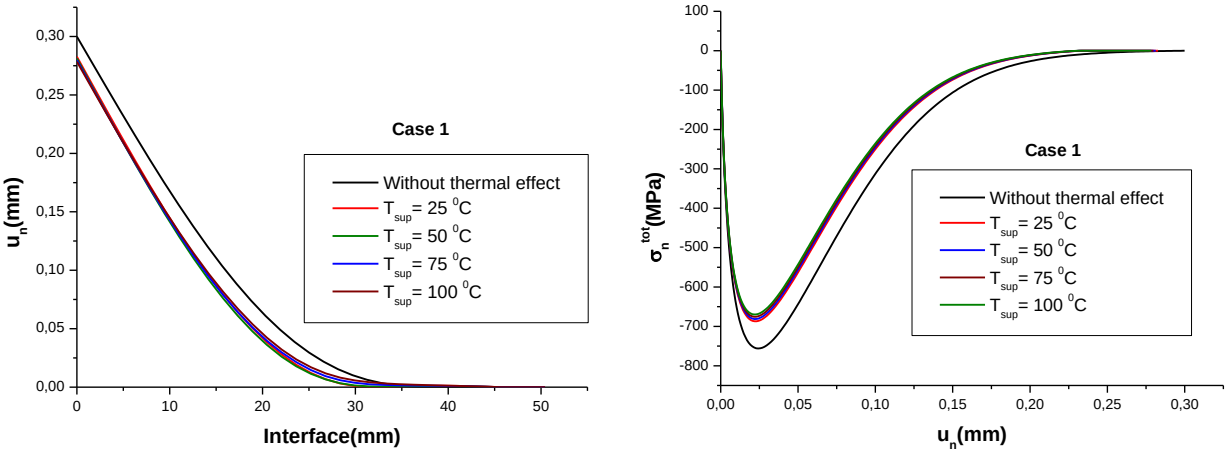

(a) (b)

Fig. 7. The normal displacement u_n along the interface and the evolution of the normal stresses σ_n^{total} at point B as a function of debonding u_n for the case 1

Table 2. Delamination behavior parameters for case 1

	Total energy dissipated w_{tot}, mJ/mm^2	Maximal total normal stress $\sigma_n^{total}{}_{max}$, MPa	Normal displacement at the maximum total normal stress, mm	Maximum normal displacement, mm
Without thermal effect	70.23225	756.144	0.02418	0.3
T_{sup}=25 °C	59.41112	687.066	0.02199	0.28274
T_{sup}=50 °C	58.61297	681.286	0.0218	0.28129
T_{sup}=75 °C	57.81588	675.507	0.02162	0.27986
T_{sup}=100 °C	56.99992	669.742	0.02262	0.27842

For the case 2, we have reported on Fig. 8(a) the normal displacement u_n along the interface with and without the thermal effect. Fig. 8(b) shows the evolution of the normal stresses σ_n^{total} at point B as a function of debonding u_n.

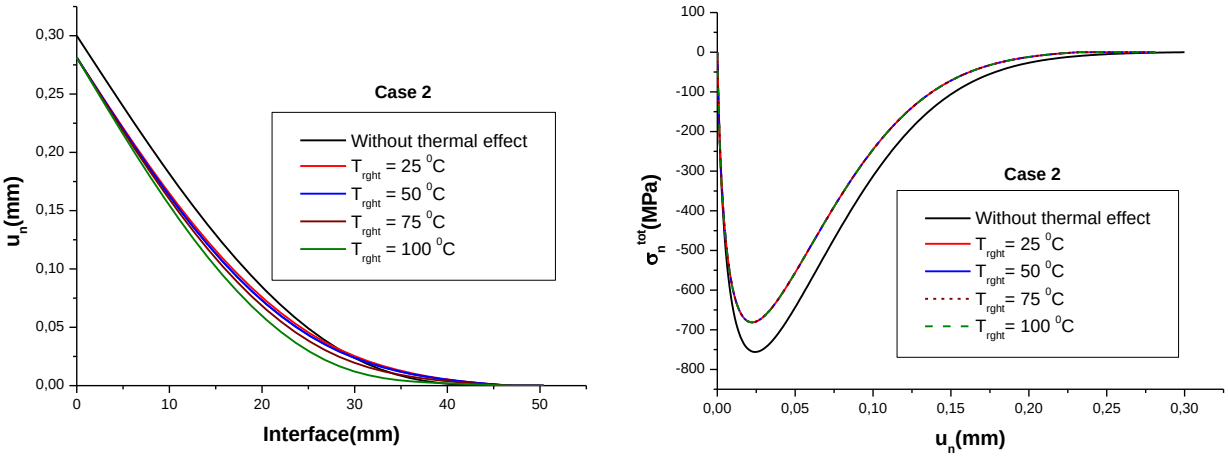

(a) (b)

Fig. 8. The normal displacement u_n along the interface and the evolution of the normal stresses σ_n^{total} at point B as a function of Debonding u_n for the case 2

The thermal field effect can be clearly observed. The behavior before decohesion is linear elastic and characterized by the value of the coefficient of initial stiffness K_{nn}, K_{tt}. For higher temperatures, the separation is weaker, but the behavior of the interface becomes more brittle, and cracking will be sharper and more advanced. The delamination of the interface remains the same for the various values of the imposed temperature T_{right}. The interface points sliding due to the dilatancy affects the total points debonding from the surfaces in contact.

It should be noted here that in all the cases treated, the temperature of the upper face dominates the distribution of the thermal field in the vicinity of the interface. Indeed, the right-side edge of the thin layer of aluminum is smaller compared to the upper face. This phenomenon is very well observed in Table 3, summarizing the delamination behavior parameters for case 2.

Table 3. Delamination behavior parameters for case 2

	Total energy dissipated w_{tot}, mJ/mm^2	Maximal total normal stress $\sigma_n^{total}{}_{max}$, MPa	Normal displacement at the maximum total normal stress, mm	Maximum normal displacement, mm
Without thermal effect	70.23225	756.144	0.02418	0.3
T_{rght}=25 °C	58.60954	681.286	0.0218	0.28129
T_{rght}=50 °C	58.61297	681.286	0.0218	0.28129
T_{rght}=75 °C	58.61375	681.286	0.0218	0.28129
T_{rght}=100 °C	58.61456	681.286	0.0218	0.28129

Parametric study. The delamination process is calculated using key interface behavior parameters such as decohesion energy (w) and initial interface stiffnesses (K_{nn}, K_{tt}). This relatively study consists in varying one of the parameters when the others are fixed. The parametric study results are presented in the form of debonding evolution un along the interface. The comparison will be carried out in the case (T_{sup} =100 °C, T_{rght} =50 °C) of the thermal effect and also without the thermal effect as shown in Fig. 9. It is clear that the delamination behavior

is strongly influenced by the initial interface stiffnesses and the decohesion energy. It can be noticed that the thermal effect is more sensitive in the case of low values of stiffness or decohesion energy. On the other hand, it becomes negligible for higher values.

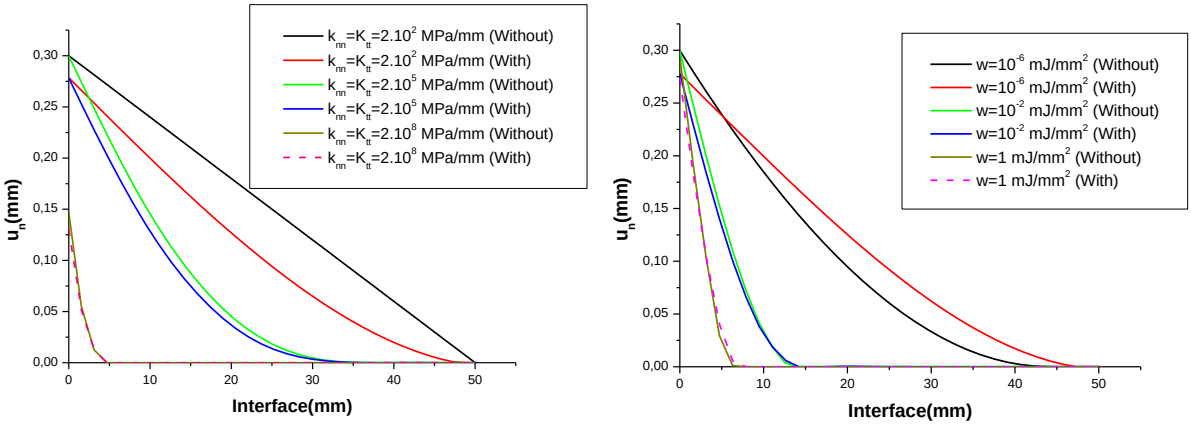

(a) (b)

Fig. 9. Influence of the interface initial stiffnesses and the decohesion energy with (a) and without (b) thermal effect

Increasing the stiffness of the interface leads to a brutal decohesion, localized over a reduced length. Likewise, an increase in the decohesion energy generates a thrust of the maximal total normal stress and the critical displacement. This leads, of course, to a delay in interface cracking. In other words, the thermal field has effects only after the damage to the interface begins, and we will have a progressive reduction of adhesive reactions.

Shear delamination of a block of aluminum

The aim of the second example is to study the role of friction in a 2D (*L*x*H*) plane strain delamination phenomena in the presence of a thermal field. In this case, an Aluminum block (Young's modulus $E = 69000$ MPa, Poisson's ratio $\nu = 0.333$, Thermal conductivity $\lambda = 230$ W/m·k and Expansion Coefficient $\alpha = 23E\text{-}6/K$) is compressed on a rigid plane under different thermal fields. At the first, the structure is completely in adhesion (D=1) and zero displacement ($u_n = 0$, $u_t = 0$). Then, the block is submitted to a vertical displacement on the upper face of block *v*, and a displacement is imposed on its left lateral edge u, with v = -0.5 mm and $u = 20$ mm in 10 s, with 210-time increments. The geometric configuration and boundary conditions are shown in Fig. 10, with $L = 50$ mm; $H = 25$ mm. The interface properties are illustrated in Table 4. In which the interface behavior is considered with dissipative law ($b \neq 0$).

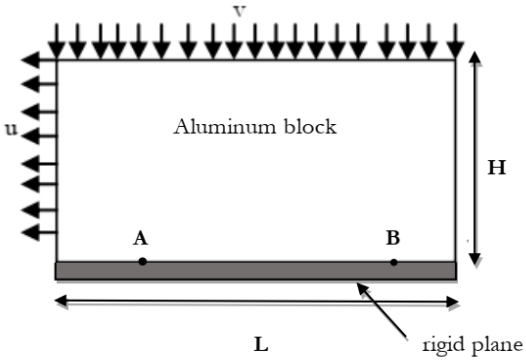

Fig. 10. Geometry and boundary conditions

Table 4. The interface properties

Properties	Decohesion energy w, mJ/mm^2	Maximal cohesive stress σ^{coh}_{max}, MPa	Initial stiffnesses of the interface K_{nn}, K_{tt}, MPa/mm	Interface viscosity b, N·s/mm	Friction coefficient μ
Interface	5.E-4	0.001	1.E+5	0.05	0.2

Mesh convergence test. Because the contact problem remains the same as in the previous example between deformable and rigid bodies, we consider the same finite element type. We discretize the domain using a linear triangular element (CPE3: A 3-node linear plane strain triangle) with a different number of elements (10, 32 and 40 elements). Figure 11 comparatively shows the results of the element numbers test in terms of the tangential sliding along the interface. We can find that the difference between element numbers is negligible, in particular in the case of 32, 40 elements. For this reason, we chose CPE3 32 elements and 33 contact nodes in the interface. The deformed meshes is shown in Fig. 12 for three-time steps t1, t2, and t3. The tangential sliding and total tangential stresses evolution along the interface in Fig. 13.

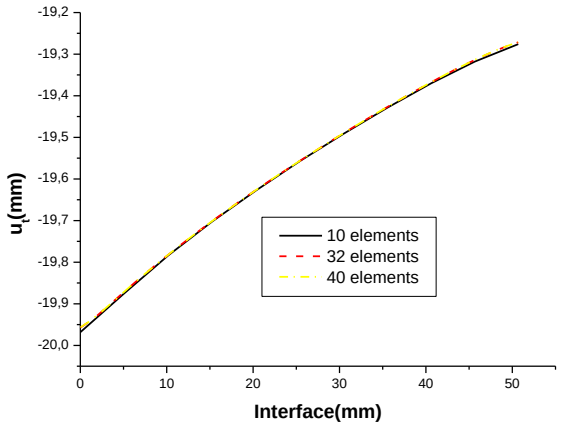

Fig. 11. The tangential sliding evolution along the interface

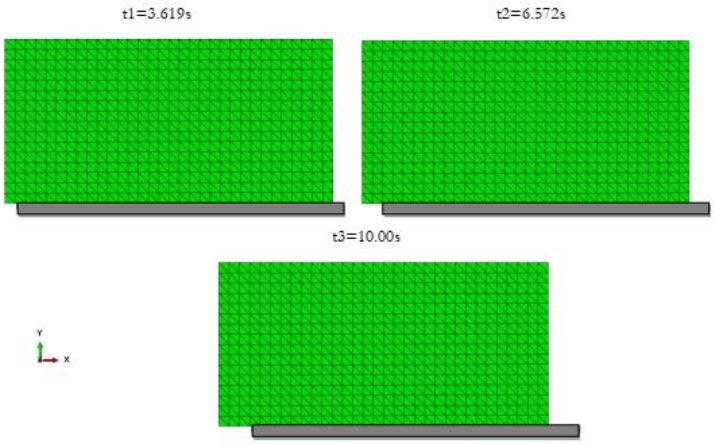

Fig. 12. The deformed meshes

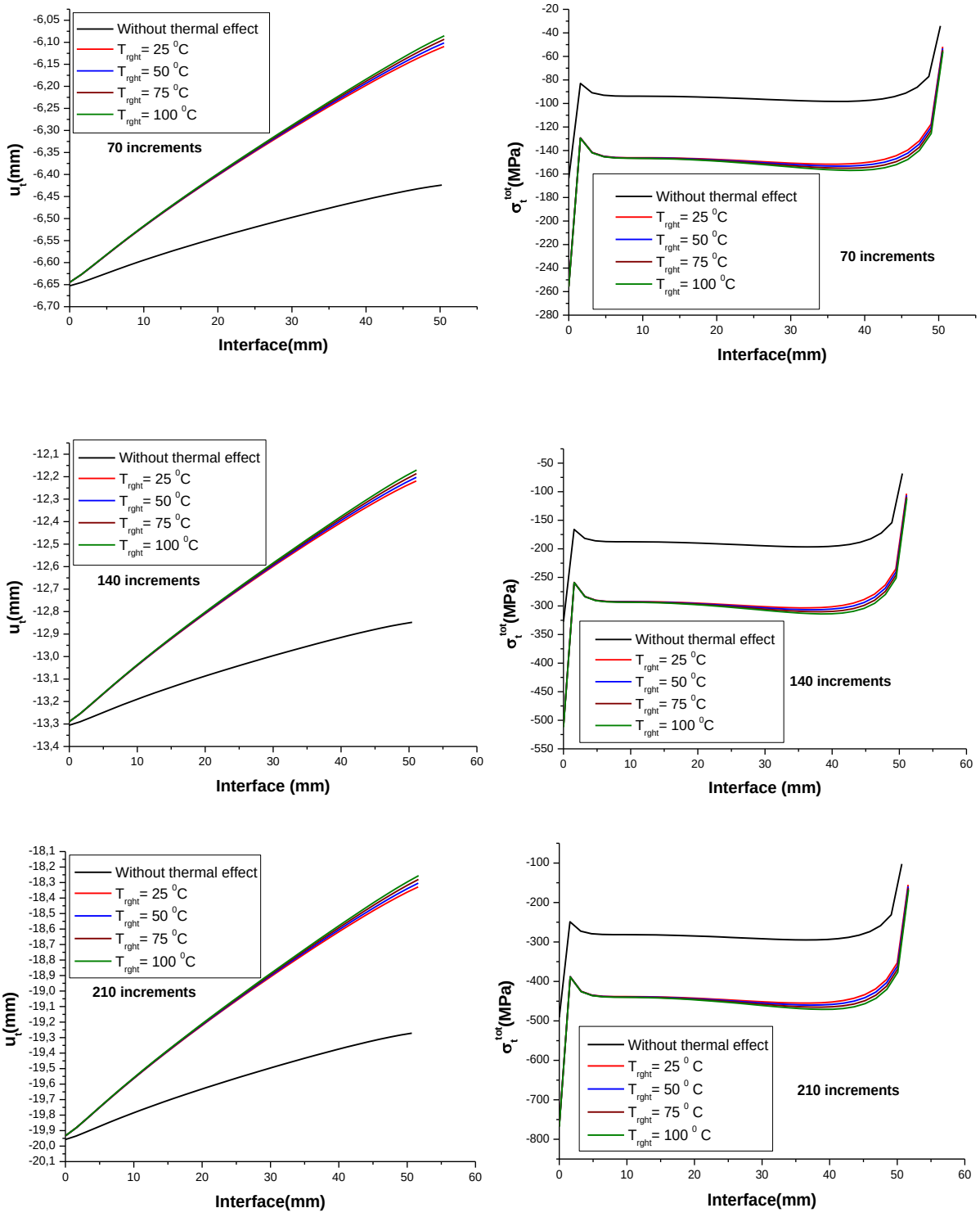

Fig. 13. The tangential sliding and total tangential stresses evolution along the interface

Temperature effect. In the thermal effect analysis, we consider the case of four states of imposed temperature on the right lateral edge of the thin layer with T_{rght} = 25, 50, 75 and 100 °C and on the upper face of the thin layer a temperature imposed constant T_{sup}=50 °C.

We begin by studying to see whether temperature affects the delamination in mode II, in terms of the total tangential stresses and tangential sliding evolution along the interface. For a more direct comparison, we use three-time increments, namely 70, 140 and 210, respectively t_1 = 3.333s, t_2 = 6.666s and t_3 =10.00s. Figure 14 shows the tangential sliding u_t and total tangential stresses σ_t^{tot} along the interface for the given times t_1, t_2, and t_3 with and without thermal effect.

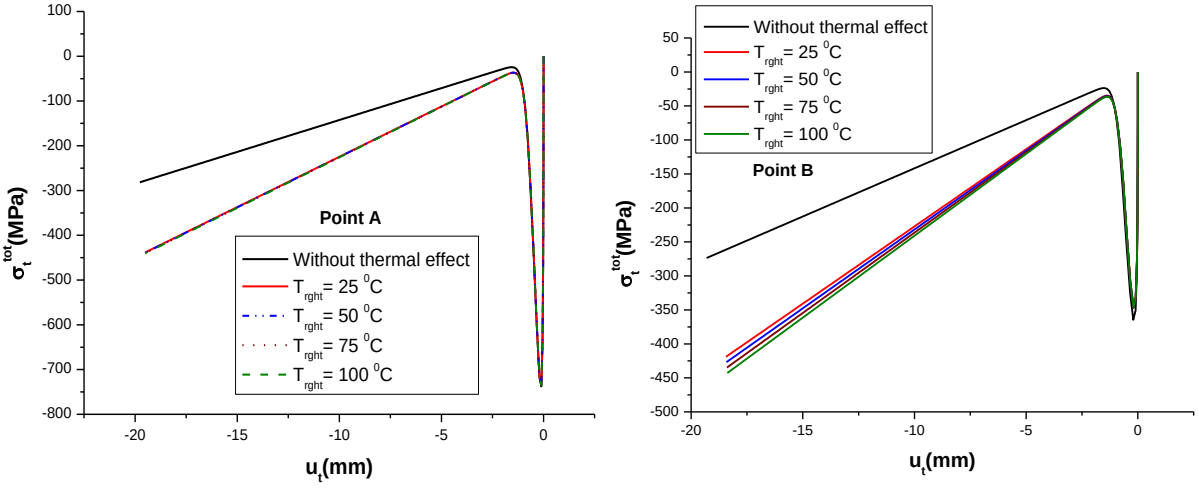

(a) (b)

Fig. 14. The evolution of the total tangential stresses σ_t^{tot} at the point as a function of tangential sliding u_t: a) Point A (at node 136); b) Point B (at node 510)

The results reveal that under the presence of a thermal field (for different imposed temperatures), the interface generates more important adhesive reactions. This results in a significant decrease in the sliding of the interface nodes.

In fact, two zones can be observed. In the vicinity of the left face and in the center of the interface, the nodes slip in the same way, whatever the imposed temperature. On the other hand, in the vicinity of the right face of the aluminum layer, where the temperatures are imposed, the behavior is different. This is mainly due to the temperature gradient concentrated in this zone.

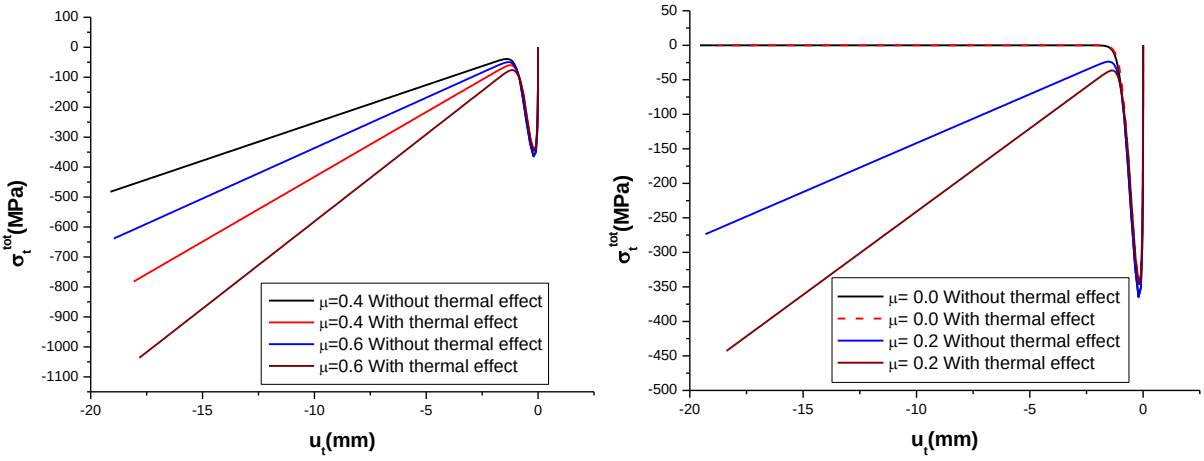

(a) (b)

Fig. 15. The evolution of the total tangential stresses σ_t^{tot} at point A as a function of tangential sliding u_t with (a) and without thermal effect (b)

In order to enrich this study, we plotted the evolution of the total tangential stresses σ_t^{tot} as a function of tangential slip u_t. For this purpose, we chose two different points of the interface: A (at node 136) and B (at node 510), as shown in Fig. 15.

Initially and under compression, the aluminum layer remains in adhesion with the rigid foundation (u_n = 0). As long as the tangential reaction is smaller than the sliding limit, the sliding does not occur. As the lateral displacement (u) progresses, an elastic sliding occurs and the slip limit is reached. At this stage, the interface generates an adhesive resistance, and the tangential behavior is elastic with damage. It should be noted here that at this stage, there is no influence of the thermal field. When the displacement is large enough, the elastic energy becomes greater than the adhesion energy limit (w) and the maximal tangential stress is reached. Then the interface damage gradually occurs, which implies a decrease in adhesive reactions until their complete disappearance, and on the other hand, friction begins to operate.

In this stage, the thermal effect is negligible except for the case of point B where there is a high temperature in which the damage initiation accelerates, expressed by the diminution of the maximal total tangential stress $\sigma_t^{tot}{}_{max}$ as shown in Fig. 15. When the adhesion is completely broken (D-1 = 0), the usual Coulomb friction conditions are obtained. It is remarked that the temperature effect is clear in the friction behavior, where there is an important sliding for the cases of high temperature compared to the other cases. Finally, it was concluded that the presence of the thermal field influences the delamination behavior in mode II significantly.

Influence of friction coefficient. As is well known, the delamination in mode II is defined by shear loads. For this reason, we study the friction effect in delamination behavior with and without thermal effect. Concerning the friction coefficient, we consider four values of μ, namely 0.0, 0.2, 0.4 and 0.6.

The thermal case considered is T_{sup} = 50 °C and T_{rght} = 100 °C at point B. Figure 15 shows the evolution of the total tangential stresses σ_t^{tot} at point B as a function of tangential sliding u_t for different friction coefficient. It can be noted that when the coefficient of friction μ increases, the decohesion threshold is slightly pushed back. However, in the presence of the thermal field, an increase in the coefficient of friction accelerates the delamination and causes significant slip. This can be justified by a large dilatancy due to the concentration of an important thermal gradient. It's clear that the effect of the presence of thermal stress is not negligible, and can influence the delamination behavior. It is therefore necessary to couple these phenomena.

Conclusions

In this research paper, the delamination behavior between an elastic body and a rigid support taking into account the thermal effect was studied. The behavior of the interface is simulated using a cohesive zone model (CZM) coupling contact, friction, and adhesion, implemented in the finite element software ABAQUS. Adhesion is regarded as interface damage is used. It is, therefore, a model which integrates the rigidity of the interface used as a parameter of damage. The variations are controlled by the displacement jumps of the nodes in contact as well as the threshold of the energy developed at the interface (Decohesion energy w).

The ability of the model is tested with a benchmark to simulate the 2D delamination behavior of the interface. Two examples, considering mode I (normal behavior) and mode II (shear behavior) have been studied in detail. Sequential stress analysis is adopted and thermal stresses are considered as external loads. The above results lead to the following conclusions:

1. In all the treated cases, it was noticed that at the beginning of the loading, the interface behavior is unaffected by the presence of the thermal field. The behavior of the interface is elastic, characterized by the stiffnesses initials K_{nn} and K_{tt}. Delamination only occurs when the elastic energy is reached a critical value (w: decohesion energy). As long as this threshold is not reached, adhesion remains total.

2. For mode I, the interface debonding decreases in the presence of the thermal field. On the other hand, the critical stress decreases, which accelerates delamination process. The interface becomes more brittle, and cracking will be sharper and more advanced. It should be noted here that the thermal field only has an effect if it has a temperature gradient in the vicinity of the interface.
3. The interface behavior is strongly influenced by the initial stiffnesses (K_{nn}, K_{tt}), and the decohesion energy (w). Indeed, the thermal effect is more sensitive in the case of low values of stiffness or energy than in the case of higher values.
4. For the case of delamination in mode II, the presence of a strong temperature gradient leads to a more difficult sliding, and thus to higher tangential reactions. On the other hand, the interface behavior is characterized by a reduction in the threshold of the total tangential stress. That means an acceleration of the damage initiation. This appeared very clear in the zone of the higher temperature gradient. We also notice great sensitivity to the friction effect in the mode II delamination behavior in particular when we take into account the thermal effect.

Finally, the thermal field effect is not negligible and can influence the delamination process. A thermomechanical study coupling the phenomenon of contact and friction with the presence of thermal stresses is, therefore, necessary.

References

1. Anderson TL. *Fracture Mechanics: Fundamentals and Applications*. CRC Press; 2017.
2. Alfano G. On the influence of the shape of the interface law on the application of cohesive-zone models. *Compos. Sci. Technol*. 2006;66(6): 723-730.
3. *Abaqus. Analysis user's manual - Versin 6.14.* Providence, RI: Dassault Systemes Simulia Corp; 2011.
4. Xu C, Siegmund T, Ramani K. Rate-dependent crack growth in adhesives: I. Modeling approach. *Int. J. Adhes. Adhes*. 2003;23(1): 9-13.
5. Dimitri R, Trullo M, Zavarise G, de Lorenzis L. A consistency assessment of coupled cohesive zone models for mixed-mode debonding problems. *Frattura ed Integrita Strutturale*. 2014;8(29): 266-283.
6. Jin ZH, Sun CT. Cohesive zone modeling of interface fracture in elastic bi-materials. *Eng. Fract. Mech*. 2005;72(12): 1805-1817.
7. Achour T, Mili F. Composite lay-up configuration effect on double and single sided bonded patch repairs. *Frattura ed Integrita Strutturale*. 2022;16(61): 327–337.
8. Alfano G, Sacco E. Combining interface damage and friction in a cohesive-zone model. *Int. J. Numer. Methods Eng*. 2006;68(5): 542-582.
9. Marfia S, Sacco E. Multiscale damage contact-friction model for periodic masonry walls. *Comput. Methods Appl. Mech. Eng*. 2012;205–208: 189-203.
10. Parrinello F, Borino G. Non associative damage interface model for mixed mode delamination and frictional contact. *European Journal of Mechanics, A/Solids*. 2019;76: 108-122.
11. Zhang J, Zhang X. Simulating low-velocity impact induced delamination in composites by a quasi-static load model with surface-based cohesive contact. *Compos. Struct*. 2015;125: 51-57.
12. Liu PF, Gu ZP, Peng XQ. A nonlinear cohesive/friction coupled model for shear induced delamination of adhesive composite joint. *Int. J. Fract*. 2016;199(2): 135–156.
13. Valente S, Alberto A, Barpi F. Sub-critical cohesive crack propagation with hydro-mechanical coupling and friction. *Frattura ed Integrita Strutturale*. 2016;10(35): 306-312.
14. Schryve M. *Modèle d'adhésion cicatrisante et applications au contact verre/élastomère*. Université de Provence - Aix-Marseille I; 2008. (In-French) Available from: https://tel.archives-ouvertes.fr/tel-00487968

15. Terfaya N, Berga A, Raous M. A bipotential method coupling contact, friction and adhesion. *International Review of Mechanical Engineering*. 2015;9(4): 341–353.
16. Terfaya N. *Modélisation de l'interaction sol pieu avec prise en compte du contact et frottement par la méthode du matériau standard implicite. Thèse de doctorat.* 2019. (In-French)
17. Raous M. Interface models coupling adhesion and friction. *Comptes Rendus Mécanique*. 2011;339(7-8): 491-501.
18. Raous M, Monerie Y. Unilateral contact, friction and adhesion: 3D cracks in composite materials. In: *Contact Mechanics*. Springer; 2002. p.333-346.
19. Raous M, Cangémi L, Cocu M. A consistent model coupling adhesion, friction, and unilateral contact. *Comput. Methods Appl. Mech. Eng*. 1999;177(3–4): 383-399.
20. Raous M, Cangémi L, Cocu M. Un modèle couplant adhérence et frottement pour le contact entre deux solides déformables. *Comptes Rendus de l'Academie de Sciences - Serie IIb: Mecanique, Physique, Chimie, Astronomie*. 1997;325(9): 503-509.
21. Li X, Marasteanu MO. Cohesive modeling of fracture in asphalt mixtures at low temperatures. *Int. J. Fract*. 2005;136: 285–308.
22. Białas M. Finite element analysis of stress distribution in thermal barrier coatings. *Surf. Coat. Technol*. 2008;202(24): 6002-6010.
23. Nikolova G, Ivanova J, Valeva V, Mroz Z. Mechanical and thermal loading of two-plate structure. *Comptes Rendus de L'Academie Bulgare des Sciences*. 2007;60(7): 735-742.
24. Chen J, Fox D. Numerical investigation into multi-delamination failure of composite T-piece specimens under mixed mode loading using a modified cohesive model. *Compos. Struct*. 2012;94(6): 2010-2016.
25. Ho SL, Joshi SP, Tay AAO. Experiments and three-dimensional modeling of delamination in an encapsulated microelectronic package under thermal loading. *IEEE Trans. Compon. Packaging Manuf. Technol*. 2013;3(11): 1859-1867.
26. Hu P, Han X, da Silva LFM, Li WD. Strength prediction of adhesively bonded joints under cyclic thermal loading using a cohesive zone model. *Int. J. Adhes. Adhes*. 2013;41: 6-15.
27. Shlyannikov V, Yarullin R, Ishtyryakov I. Effect of different environmental conditions on surface crack growth in aluminum alloys. *Frattura ed Integrita Strutturale*. 2017;11(41): 31-39.
28. Zhou H, Gao WY, Biscaia HC, Wei XJ, Dai JG. Debonding analysis of FRP-to-concrete interfaces between two adjacent cracks in plated beams under temperature variations. *Eng. Fract. Mech*. 2022;263:108307.
29. Rabinovitch O. Impact of thermal loads on interfacial debonding in FRP strengthened beams. *Int. J. Solids Struct*. 2010;47(24): 3234-3244.
30. Im JM, Kang SG, Shin KB, Hwang TK. Prediction of onset and propagation of damage in the adhesive joining of a dome-separated composite pressure vessel including temperature effects. *Int. J. Precis. Eng. Manuf.* 2017;18(12): 1795–1804.
31. Jiang J, Wang W, Zhao X, Liu Y, Cao Z, Xiao P. Numerical analyses of the residual stress and top coat cracking behavior in thermal barrier coatings under cyclic thermal loading. *Eng. Fract. Mech*. 2018;196: 191-205.
32. Na J, Mu W, Qin G, Tan W, Pu L. Effect of temperature on the mechanical properties of adhesively bonded basalt FRP-aluminum alloy joints in the automotive industry. *Int. J. Adhes. Adhes*. 2018;85: 138-148.
33. Zhong YL, Gao L, Wang P, Liang SJ. Mechanism of interfacial shear failure between crts II slab and ca mortar under temperature loading. *Engineering Mechanics*. 2018;35(2): 230-238.
34. He J, Xian G, Zhang YX. Effect of moderately elevated temperatures on bond behaviour of CFRP-to-steel bonded joints using different adhesives. *Constr. Build Mater*. 2020;241: 118057.

35. Chen X, Zhu Y, Cai D, Xu G, Dong T. Investigation on interface damage between cement concrete base plate and asphalt concrete waterproofing layer under temperature load in ballastless track. *Appl. Sci*. 2020;10(8): 2654.
36. Katafiasz TJ, Greenhalgh ES, Allegri G, Pinho ST, Robinson P. The influence of temperature and moisture on the mode I fracture toughness and associated fracture morphology of a highly toughened aerospace CFRP. *Compos. Part A Appl. Sci. Manuf*. 2021;142: 106241.
37. Cui X, Du B, Xiao H, Zhou R, Guo G, Liu H. Interface damage and arching mechanism of CRTS II slab track under temperature load. *Constr. Build. Mater*. 2021;291: 123258.
38. Guo D, Zhou H, Wang HP, Dai JG. Effect of temperature variation on the plate-end debonding of FRP-strengthened steel beams: Coupled mixed-mode cohesive zone modeling. *Eng. Fract. Mech*. 2022;270: 108583.
39. Gong Y, Jiang L, Li L, Ren S, Zhao Y, Wang Z, Hu N. Temperature effect on the static mode I delamination behavior of aerospace-grade composite laminates: Experimental and numerical study. *Fatigue Fract. Eng. Mater. Struct*. 2022;45(10): 2827-2844.
40. Truong VH, Hoang VT, Choe HS, Nam YW, Kweon JH. Delamination growth in curved composite beam at elevated temperatures. *Advanced Composite Materials*. 2022;31(2): 151-172.
41. Attarian S, Xiao S. Investigating the strength of Ti/TiB interfaces at multiple scales using density functional theory, molecular dynamics, and cohesive zone modeling. *Ceram. Int*. 2022;48(22): 33185-33199.
42. Rahbar-Rastegar R, Dave EV, Daniel JS. Fatigue and thermal cracking analysis of asphalt mixtures using continuum-damage and cohesive-zone models. *Journal of Stomatology*. 2018;144(4).
43. Erdogan F, Wu BH. Crack problems in FGM layers under thermal stresses. *Journal of Thermal Stresses*. 1996;19(3): 237-265.
44. Chen WQ. Some recent advances in 3D crack and contact analysis of elastic solids with transverse isotropy and multifield coupling. *Acta Mechanica Sinica*. 2015;31(5): 601–626.
45. Terfaya N. *Contribution à la modélisation des problèmes de contact et de frottement bi–dimensionnels. Génération de maillage et programmation orientée-objet de la méthode des éléments finis. Mémoire de Magister*. Algérie: CU Béchar; 2000;
46. Raous M. Quasistatic Signorini problem with Coulomb friction and coupling to adhesion. In: *New developments in contact problems*. Springer; 1999. p.101–178.
47. Chabrand P, Dubois F, Raous M. Various numerical methods for solving unilateral contact problems with friction. *Math. Comput. Model*. 1998;28(4–8): 97-108.
48. Wriggers P, Laursen TA. *Computational Contact Mechanics*. Springer; 2006.
49. Monerie Y. *Fissuration des matériaux composites : rôle de l'interface fibre/matrice*. Universite Aix-Marselle II; 2000.
50. Elices M, Guinea GV, Gómez J, Planas J. The cohesive zone model: Advantages, limitations and challenges. *Eng. Fract. Mech*. 2001;69(2): 137-163.
51. Dugdale DS. Yielding of steel sheets containing slits. *J. Mech. Phys. Solids*. 1960;8(2): 100-104.
52. Barenblatt GI. The Mathematical Theory of Equilibrium Cracks in Brittle Fracture. *Advances in Applied Mechanics*. 1962;7: 55-129.
53. Park K, Paulino GH. Cohesive zone models: A critical review of traction-separation relationships across fracture surfaces. *Appl. Mech. Rev*. 2011;64(6): 060802.
54. Chaboche JL, Feyel F, Monerie Y. Interface debonding models: A viscous regularization with a limited rate dependency. *Int. J. Solids Struct*. 2001;38(18): 3127-3160.

THE AUTHORS

Abdellah Benchekkour
e-mail: benchekkour.abdellah@univ-bechar.dz

Nazihe Terfaya
e-mail: terfaya.nazihe@univ-bechar.dz

Mohammed Elmir
e-mail: elmir.mohammed@univ-bechar.dz

Tayeb Kebir
e-mail: kebirtayeb@live.fr

Mohamed Benguediab
e-mail: benguediabm@gmail.com